Belnoue, J. P., Nixon-Pearson, O. J., Ivanov, D., & Hallett, S. R. (2016). A Novel Hyper-Viscoelastic Model for Consolidation of Toughened Prepregs under Processing Conditions. Mechanics of Materials, 97, 118-134. DOI: 10.1016/j.mechmat.2016.02.019

University of Bristol - Explore Bristol Research
General rights

CrossMark
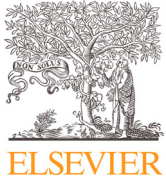
A novel hyper-viscoelastic model for consolidation of toughened prepregs under processing conditions

J.P.-H. Belnoue*, O.J. Nixon-Pearson, D. Ivanov, S.R. Hallett

Advanced Composites Center for Innovation and Science (ACCIS), University of Bristol, Queen's Building, Bristol BS8 1TR, United Kingdom

ABSTRACT

The paper presents a new modelling concept for describing the compressibility of toughened uncured prepregs over a wide range of processing conditions (i.e. automatic fibre deposition, hot debulking and pre-curing consolidation). The primary challenge of the work is to simulate the material response due complex flow and deformation mechanisms. This generation of prepreg systems exhibits both percolation (bleeding) flow typical for conventional thermosets, where the pressure gradient causes resin flow relative to the fibres, and shear (squeezing) flow typical for thermoplastics, where the laminate behaves as a highly viscous incompressible fluid. As a result, it holds features of both the systems: e.g. a convergence to a certain compaction limit at high temperatures and pressure levels and size/ply configuration-dependent material response. The modelling starts from microstructural considerations, which give the foundation for an analytical model that assumes a transition from percolation to shear flow. It is shown that this model can capture the material behaviour very well. A hyper-viscoelastic material model is then constructed and implemented within the finite element package Abaqus/Standard. The model parameters are identified from an experimental programme and validated against compaction experiments over a wide range of load rates, temperatures and laminate configurations.

1. Introduction

The increasing use of composite material attracts attention to the idea of replacing the traditional (costly) experimental trial-and-error based methods with the optimisation of processing parameters through numerical simulations and virtual manufacturing. The increasing complexity of component geometries together with the development of new manufacturing techniques (e.g. automatic fibre placements and automatic tape lay-up) and new prepreg systems (e.g. toughened systems) have created the need for new numerical models able to adequately describe the physical complexity of the

manufacturing processes. One of the key steps in the manufacturing processes is the consolidation/compaction of composite prepregs prior to curing. In broad terms, consolidation is commonly understood as the processing step in which pressure is applied and plies are engaged in a full contact and inter- and intra-ply porosity is eliminated by means of compaction. The present paper focuses on the thickness evolution of the prepreg stacks associated with consolidation. It is essential because it (a) determines the component dimensions; (b) the formation of fibre path defects is often a direct consequence of excess fibre length generation at this stage, which may result in features such as wrinkling, folds, and in-plane waviness. Thus, the compressibility of prepregs, which is determined predominantly by resin flow within a dense fibre network, strongly influences the quality of the final part.

* Corresponding author. Tel.: +44 1173315798.
  E-mail address: jonathan.belnoue@bristol.ac.uk (J.P.-H. Belnoue).

Modern prepreg systems are often toughened with thermoplastic particles either in the form of interleaves in between plies or distributed within the inter-fibre space. Inter-ply cracks in toughened laminates are forced to follow a more torturous path and hence this increases mode II fracture toughness, compression after impact and other crucial composite properties. Alongside improvements in mechanical performance it also significantly affects flow mechanisms by making the resin more viscous. This, in turn, affects the morphology of interfaces, inter-ply interaction, cure kinetics, etc. Hence, it is crucial to understand the behaviour of these materials in relation to their internal structure and the properties of their constituents. In the typical temperature range of deposition and consolidation used in manufacturing (~30–90 °C), interleaved prepregs exhibit a strong variation in viscosity -up to six orders of magnitude (Lukaszewicz, 2011). Viscosity determines the flow type: the resin can either escape from the ply without shifting the fibres (known as bleeding or percolation flow), or push fibres transversely making the system deform as an incompressible fluid (known as squeezing or shear flow). Toughened thermosets, within the temperature range used, exhibit intermediate viscosity, where a concurrent flow pattern is observed. As a result, toughened prepregs exhibit features typical of both traditional low-viscosity thermosets and traditional high viscosity thermoplastics.

The flow mechanism at the fibre and ply scale determines the ability of the material to deform in consolidation processes. In pure bleeding the through-thickness compaction is limited, determined by the ratio of initial fibre volume fraction (typically 40–50% after debulking) to the maximum fibre volume fraction (typically 70–75%). In the squeezing flow higher overall compressibility is possible due to the transverse flow of material. Understanding the transition between these flows is essential. For instance, heating to an elevated temperature prior to consolidation may forbid the closure of gaps between tows: the resin bleeds out rather than pushes fibres into those gaps. On the other hand, consolidation at low temperatures can require unrealistically high pressure levels to achieve a certain thickness.

An early review of the flow models for prepregs was conducted by Hubert and Poursartip (1998). Engmann et al. (2005) produced a comprehensive summary of squeezing flow models for isotropic fluids. Among the rich variety of the available compaction models, analytical models present a particular interest for this study since they allow for the direct identification of material properties (from simple compaction tests). The first analytical solution, relating applied pressure to thickness for an ideal unidirectional fibre reinforced Newtonian fluid under no-slip and zero-friction conditions, was obtained by Rogers (1989). This solution was later generalised to account for ply interaction (Kaprielian and O'Neil, 1989), partial slip (Balasurbramanyam et al., 1989), and rate-dependent material response such as a shear thinning power law (Wang and Gutowski, 1991). More complex forms of material behaviour, for example the Carreau-type, present a serious challenge for analytical integration (Shuler and Advani, 1996). Servais et al. (2002), considering Newto-

nian and Power Law as the limit cases of Carreau and Herschel–Bulkley behaviour, suggested a closed form solution for stochastically reinforced media. Squeezing flow models have been mostly applied to and validated against highly viscous thermoplastics such as PEEK, PS (Wang and Gutowski, 1991; Shuler and Advani, 1996), and PP (Servais et al., 2002).

The approaches used for the description of low viscosity thermosetting resin systems are notably different. Typically percolation flow models utilise Darcy's law to describe the movement of resin and the rate-independent compaction model of fibrous networks to link pressure and the fibre volume fraction evolution (Gutowski et al., 1987; Hubert and Poursartip, 2001; Kelly et al., 2006; Gu et al., 2006; Li and Tucker, 2002). Considering the compaction of prepreg saturated with liquid resins, Hubert and Poursartip (2001) demonstrated that the rate independent constituent of material reaction (fibre bed response) does not depend on the ply lay-up and laminate thickness. Commonly used additive superposition of viscous and elastic responses leads to differential equations, which show gradual pressure redistribution from resin to fibre network in the course of compaction. An alternative argument is presented by Kelly (2011) who demonstrated that for some material systems, such as short fibres impregnated with low viscosity resins, multiplicative stress superposition is better suited for the modelling of consolidation experiments. It is interesting to note that this idea conceptually agrees with the squeezing flow theories, where the apparent response of deformed media presents a product of elastic and viscous parts.

As shown above, most of the percolation and shear flow models are based on incompatible assumptions with regard to compressibility, fibre movement, and resin flow. Since these models have traditionally been applied to different classes of materials the need for a transitional model has rarely been noted. Yet there are distinct experimental data showing that a transitional model is needed. For example Hubert and Poursartip (2001), testing toughened and low viscosity prepregs on curved tools with bleed and non-bleed bagging conditions, clearly demonstrated that both squeezing and percolation flows can act concurrently. Neglecting one or another may lead to significant error in thickness estimation. Later, performing compaction experiments on uncured prepreg under different conditions of temperature, pressure and pressure rate, Ivanov et al. (2013) highlighted that toughened prepregs hold features of both thermosets- and thermoplastic-based systems. For instance, like thermoset-based systems a compaction limit phenomenon is observed, while similar to thermoplastic-based prepregs they show a size dependency and shear thinning behaviour for some sample configurations. Nixon-Pearson et al. (submitted for publication), (2015) conducted a series of compaction experiments on toughened systems over a wide range of processing conditions. The results of this study are briefly summarised in Section 2 as they form the main validation case for the models presented in this paper. The experimental observations indicate that a new formulation of the prepreg compaction material model is required. The coupling of squeezing and bleeding flow in application to prepregs systems has rarely been discussed in the literature and the

available models cannot be readily adopted. Squeezing flow theories predict the existence of the dependency of the prepreg's ability to compact on specimen width and thickness but cannot capture any compaction limit other than zero-thickness. Bleeding flow theories (that use Darcy's law), on the other hand, can capture the compaction limit but cannot take account of the effect of the material's dimension and constraints on the final (i.e. consolidated) thickness. A new material description should therefore be able to:

1. describe samples of arbitrary thicknesses by the same governing equation(s)
2. explicitly include the geometrical size effects in the formulation
3. capture the compaction limits both for squeezing and bleeding material states
4. incorporate a criterion for the switch from squeezing to bleeding flow (the existence of which is discussed further below)
5. take into account the stain-rate dependency
6. employ material constants that can be derived from the compaction tests
7. be implementable in a finite element framework.

Above all the model has to give clear route for extraction material properties.

The current paper focuses on the modelling of prepreg volumes with finite width-to-thickness ratios that are characteristic for materials produced by AFP, tapered and shape transition regions. The width-to-thickness ratio is explicitly included in the model and thus the predictions can be made for a range of geometry parameters. The model does not attempt to describe the deformation of continuous, wide prepreg sheets - under no bleed conditions the consolidation of this material is only possible at the expense of bleeding of the resin into the pores left after debulking. From the analysis of the pore volume fraction (Nixon-Pearson et al., 2015) this can be limited to 5%. The application of this prepreg consolidation model is for thickness evolution in debulking and autoclave processes where the in-plane movements of the material are relatively small compared to forming processes.

The present contribution aims at setting up a new modelling framework for resin flow in uncured toughened prepreg systems that follow all the criteria listed above. A criteria for the transition from shear flow to resin bleeding is proposed. It is further assumed that after the transition a change of direction of the resin flow between the fibres takes place, from transverse squeezing to bleeding along the fibres (which is represented as squeezing along the fibres). The form of the proposed solution is that, for each temperature, only three parameters are needed for input. The results agree well with the experimental results obtained from compaction experiments (Nixon-Pearson et al., submitted for publication, 2015). The proposed model was further implemented in the implicit finite element (FE) software Abaqus/Standard in the form of a hyper-viscoelastic model using the thermodynamical framework proposed by Limbert and Middleton (2004).

2. Brief summary of experimental results

Traditional compaction experiments (Hubert and Poursartip, 2001) aim at reproducing the boundary conditions seen by a point situated at the middle of a large flat panel. Edge effects are completely neglected and the edges of the prepreg stacks are fully constrained. The present set of experiments, on the other hand, explores the behaviour of uncured prepreg situated near the edges of a structure or, more generally, in areas where manufacturing defects are formed (i.e. areas where a lot of ply movement occurs, with a large number of shorter plies and/or ply drop-offs). To this end, the ply edges are left unconstrained which also allows them to be used to build a material model that works for arbitrary boundary conditions. The material testing took the form of a series of compactions tests conducted on crucifix shape samples (see Fig. 1). The excess fibre length in the plies was allowed to prevent the lateral loss of material from the gauge section edges of the central square pressurised area as the plies are squeezed in the through-thickness direction. Each sample was a block of 16 plies. Particular attention was given to the effect of the specimen geometry and constraints. 2 different in-plane dimensions (i.e. baseline – 15×15 mm; and scale-up – 30×30 mm) and 3 stacking sequences (i.e. cross-ply (CP) – $[90/0]_8$; semi-blocked ply (SB) – $[90_2/0_2]_4$; and blocked ply (BP) – $[90_4/0_4]_2$) were considered.

Specimens were loaded in two regimes: a slow monotonic loading, and a ramp-dwell regime where the fast application of load (consistent with AFP deposition) is followed by long creep intervals. In both these cases baseline specimens were loaded to 60 N in 1200 s, although the ramp-dwell program included five steps with an increment in load of 10 N, starting with 20 N at the first step. For scale-up specimens, the specimens were loaded to 240 N in 1200 s. The scaled up ramp-dwell program had a load increment of 40 N, starting with 80 N at the first step. Temperatures ranging from 30 °C to 90 °C were considered. Two aerospace grade toughened prepreg systems developed by Hexcel® were investigated: IM7-8552 (where thermoplastic particles are dissolved within plies throughout the bulk phase of the resin) and IMA-M21 (where an extra fraction of thermoplastic particles is preserved as a distinct interlayer between the plies during processing). All the tests were performed within the range of temperatures and time scales where the degree of cure does not evolve (maximum temperature 90 °C and test duration did not exceed 15 min). As has been shown by Hubert et al. (2001) in an isothermal test at 110 °C, considerable change in viscosity of 8552 resin only occurs after much longer times than those of the experiments presented here (i.e. above 60 min). The nature of M21 resin does not differ greatly from 8552. The thermoplastic particles melt at about 180 °C, so it seemed reasonable to assume that in the temperature range studied here, both the systems exhibit no curing.

Although not to the same extent, both material systems tested showed a significant difference in their compaction behaviour between samples with different stacking sequence. It can be seen, in Fig. 2, for the IM7-8552 material that comparing the post-compaction widths (whilst
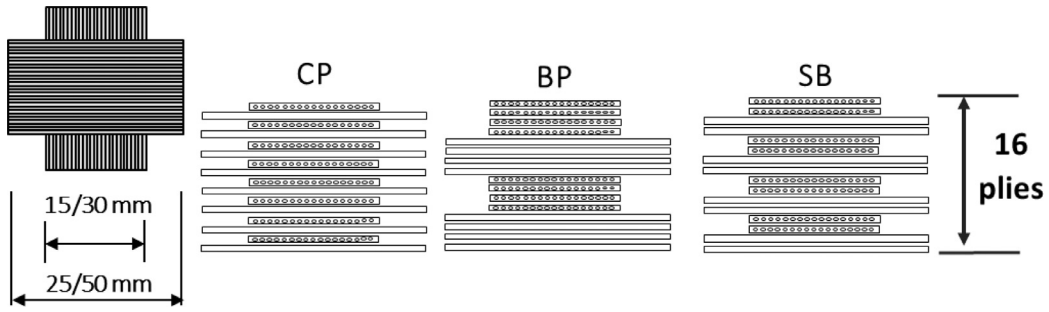
Fig. 1. Schematic representation of the CP, SB and BP specimens.

neglecting any elastic response), the CP specimens (i.e. thin plies) showed only minimal increase in width, whereas BP specimens showed a notable increase in width at temperatures over 50 °C, reaching a plateau around 70 °C; similarly, the thickness time curves (see Fig. 2(b)) reveal that at each tested temperature, BP samples are significantly more compressible than CP specimens. Moreover, past 70 °C, the samples seem to reach a compaction limit that cannot be exceeded with a further increase of the temperature. A similar trend was observed between the larger scale-up specimens and the baseline. Finally, as illustrated in Fig. 3, an evaluation of the microstructure as well as measurement of individual ply widths gave very clear evidence of the presence of both squeezing flow (through inter-ply distortion between ply-blocks) and bleeding flow (at the specimen edges).

3. A new phenomenological model for uncured toughened UD prepreg under processing conditions

3.1. Phenomenological model

In this section, a new phenomenological model for consolidation of toughened pre-preg is proposed. One of the main outcomes from the experimental program is that the material systems considered here presents features typically associated with squeezing flow (e.g. the

variation of the material response with the tape width and thickness) and also some characteristics that are usually related to percolation flow theories (e.g. the convergence to a compaction limit). Unlike traditional viscosity models for UD composites (Rogers, 1989; Wang and Gutowski, 1991; Shuler and Advani, 1996; Hubert and Poursartip, 2001; Hubert et al., 1999; Christensen, 1993; Pipes, 1992), it is hypothesised here that both flow mechanisms are present simultaneously. Existing squeezing and bleeding flow models cannot be directly combined due to the incompatible assumptions with regard to compressibility, fibre movement, and resin flow.

The pressure–thickness relations can be obtained analytically for squeezing no-slip flow of Newtonian and power-law fluids (see for example Rogers, 1989; Wang and Gutowski, 1991 or Shuler and Advani, 1996). The relation between applied pressure σ and resultant through-thickness strain rate $\dot{\varepsilon}$ (called apparent viscosity η_{app} here) can be presented as the product of a strain-dependent (η_{strain}) and a strain rate-dependent (η_{rate}) term. A summary of solutions from literature, written in terms of η_{strain} and η_{rate}, is shown in Table 1 where w_0 is the width of the UD tape/ply before compaction and η_{micro} is the viscosity of unidirectional fibre reinforced fluid (Rogers, 1989), that relates the transverse shear stress (τ) and the shear rate ($\dot{\gamma}$) at a point as: $\tau = \eta_{micro}\dot{\gamma}^n$. On the other hand, traditional percolation flow models
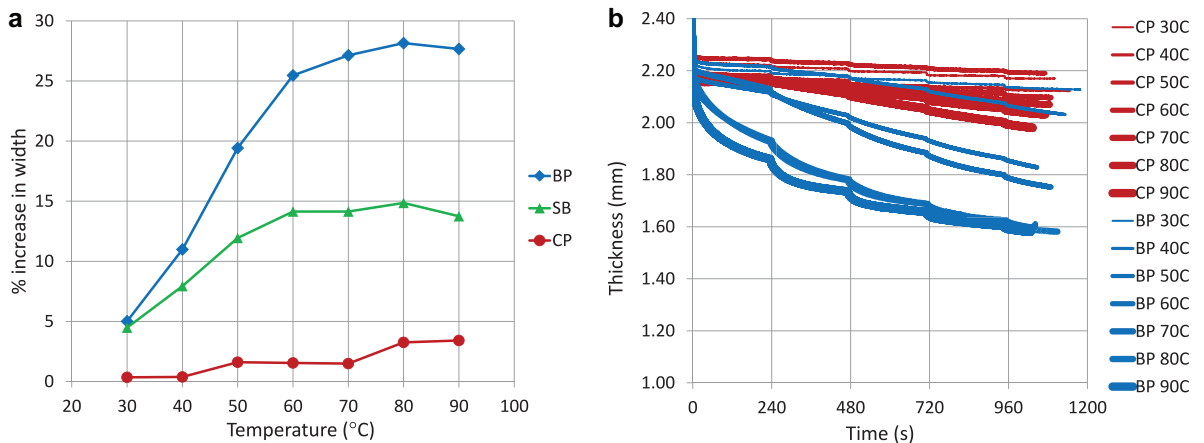

Fig. 2. (a) Increase in width vs. Temperature for material system IM7/8552. (b) – Thickness vs. time curves for BP and CP specimens for material system IM7/8552 (from Nixon-Pearson et al., submitted for publication, 2015).
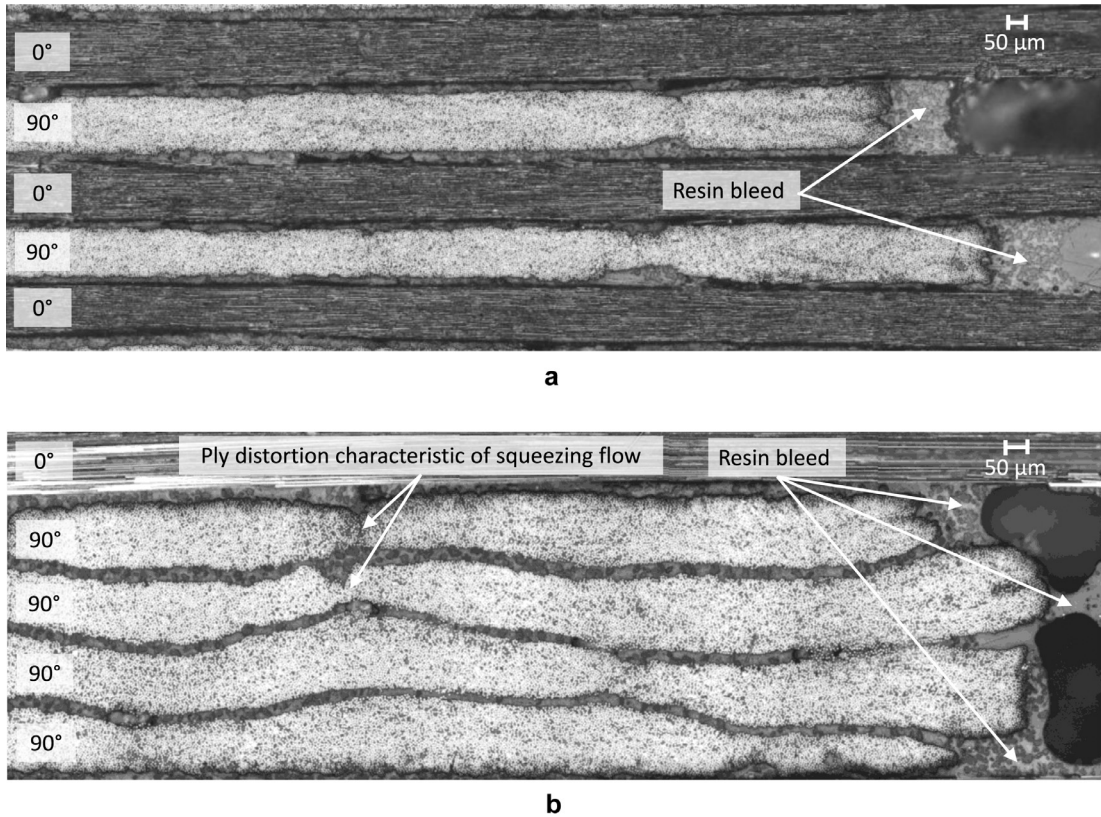
Fig. 3. Micrographs of the edge of a CP (a) and a BP (b) specimen made of IMA-M21 and tested at 90 °C. Significantly more squeezing flow (in the form of lateral fibre movement) is observed in "thicker" samples.

Table 1
Summary of some of the analytical expressions derived from Rogers (1989), Wang and Gutowski (1991) and Kelly (2011) for the apparent material response of a fibre reinforced fluid.

	η_{rate}	η_{strain}
Newtonian fluid, volume of squeezing fluid under loading plates remains constant, no-slip conditions (Rogers, 1989)	1	$\eta_{micro}(\frac{w_0}{h_0})^2\exp(-2\varepsilon)$
Power law fluid (Wang and Gutowski, 1991)	$f(n)\dot{\varepsilon}^{n-1}$	$\eta_{micro}(\frac{w_0}{h_0})^{n+1}\exp(-\varepsilon(n+1))$
Percolation flow of Kelly (2011)	A polynomial function of fibre volume fraction (or equivalently through-thickness strain).	Interpolates between stress level at very slow and very high strain rates at a given strain level

(Hubert et al., 2001) make use of Darcy's law, where the apparent viscosity is decomposed as the sum of a viscous (i.e. strain rate dependent) and an elastic term (i.e. strain dependent). More recently, Kelly (2011) proposed an empirical expression where a multiplicative decomposition of the apparent viscosity of the fibre reinforced fluid is used to describe percolation flow (see Table 1). This form of the apparent viscosity could describe the compaction response of some preforms better than the additive superposition of the terms. This motivates the choice of the formulation of a viscosity model where shear and percolation flow coexist. This viscosity presents a multiplicative decomposition of a strain and a strain rate dependent term or, equivalently, elastic and viscous parts:

$$\sigma = \eta_{app}(\varepsilon,\dot{\varepsilon})\dot{\varepsilon} = \eta_{strain}(\varepsilon)\eta_{rate}(\dot{\varepsilon})\dot{\varepsilon} \tag{1}$$

where σ is the Cauchy stress, $\varepsilon = \ln(\frac{h}{h_0})$ is the Hencky measure of strain, $\dot{\varepsilon} = \frac{\dot{h}}{h}$, and h_0 and h are the initial thickness and current thickness of the UD tape/ply, respectively.

For simplicity sake, it is assumed that η_{rate} follows a simple power law function (Wang and Gutowski, 1991; Shuler and Advani, 1996; Pipes, 1992):

$$\eta_{rate}(\dot{\varepsilon}) = e^{\bar{b}}(-\dot{\varepsilon})^a \tag{2}$$

where a and $\bar{b}$ are material parameters that need to be experimentally determined.

The formulation of the strain dependent term, η_{strain}, builds on experimental observations. The material response appears to be sensitive to the initial dimensions of the tape. Within a certain range of dimensions, scaling the samples in the plane of plies or out of plane (by

blocking plies together) changes the compressive response and flow characteristics of material (Nixon-Pearson et al., submitted for publication, 2015). These scale effects are related to the squeeze flow at the onset of deformation. At higher strain levels, however, a limit to the transverse deformation is observed, which is not described by classical squeeze flow theories (see Fig. 2). The expansion in the transverse direction gets locked-up on reaching a certain deformation level. The locking phenomena were first discussed by Wang and Gutowski (1991) for thermoplastics, who suggested that a twist of misaligned fibres at the flow front due to shear deformations blocks the transverse spreading. For all temperatures studied in the experimental investigation, thin CP samples show little transverse expansion and reach a compaction limit early in the deformation process; while transverse expansion in thicker ply samples (i.e. BP) is much higher.

In the proposed model a transition between squeezing flow and bleeding flow is considered as an instantaneous event that occurs when shear deformations at the edges reaches a critical level (ε^l). This hypothesis is introduced for simplicity and robustness of the model.

The strong scale effects observed experimentally and predicted by squeezing flow theories (Rogers, 1989) result from the non-homogeneous distribution of the deformation within the ply (Fig. 4). This non-uniformity may be a consequence of the no-slip (i.e. non-zero friction) conditions at the ply interfaces. Shear strain is high at the ply-tool interface close to the expanding ply edges, but decays to zero at the ply mid-plane, due to the deformation symmetry. At the laminate mid-plane the material is subjected to pure hydrostatic compression, and the maximum in-plane expansion and through-thickness reduction takes place in the centre of the sample's cross-section. The current model aims at a phenomenological description of ply deformation, i.e. the deformations are not considered at sub-ply level, which would require high resolution modelling with a large number of elements through the thickness and an associated high computational expense. Instead, the non-homogeneous distribution of the deformations through the ply thickness is taken in an average sense. This implies that the stress state within a tape/ply is considered uniform (Fig. 4). The ply is subjected to through-thickness compaction and in-plane spreading, as opposed to modelling the pure shearing taking place at a material point.

As the experimental data does not show any step change associated with the change in flow mode, it is important to ensure a smooth transition between the two flow regimes. In the suggested model, the geometrical locking and subsequent bleeding flow are connected through an evolution of η_{strain}, which is dependent on fibre rearrangement. The advantage of the chosen form of constitutive equations is that the transition to bleeding can, as will be shown below, be implemented consistently – using the same general form of pressure–thickness relations throughout the entire process by varying parameters describing bleeding and squeezing process. The strain dependent term has to contain structural information about the ply dimensions (ply scale geometry) as well as to take into account the flow at the fibre scale, particularly for the de-

scription of the bleeding flow, which dictates the evolution of resistance with a change in the fibre volume fraction. It was found convenient to present the strain-dependent term η_{strain} in Eq. (1) as the product of a term accounting for the deformation observed at the higher (ply) scale (η_{ply}) and of a term accounting for the deformation observed at the lower (micro) level (η_{micro}). This consideration leads to the re-formulation of Eq. (1) as:

$$\sigma = \eta_{app}(\varepsilon, \dot{\varepsilon})\dot{\varepsilon} = \eta_{strain}(\varepsilon)\eta_{rate}(\dot{\varepsilon})\dot{\varepsilon} = \eta_{micro}(\varepsilon)\eta_{ply}(\varepsilon)\eta_{rate}(\dot{\varepsilon})\dot{\varepsilon}$$
(3)

η_{ply} can be determined from rearranging Rogers' analytical solution (Rogers, 1989). A ply of dimensions h_0 and w_0 is considered. Before locking, the squeezing flow is incompressible i.e. the strain in transverse direction is equal and opposite to the strain in the compaction direction. After locking, the ply is assumed to be fully compressible i.e. no transverse expansion and the volume is lost in bleeding flow:

$$\eta_{ply} = 2\left(\frac{w_0}{h_0}\right)^2 \exp\left(-4\varepsilon\right) \qquad (a)$$

$$\eta_{ply} = 2\left(\frac{w_0}{h_0}\right)^2 \exp\left(-2\left(\varepsilon + \varepsilon^l\right)\right) \qquad (b) \qquad (4)$$

Due to the squeezing flow non-uniformity, different material points within the ply/tape do not reach locking at the same time. As a result, the flow non-uniformity is preserved after locking and the term η_{ply} remains when bleeding occurs. The remaining term η_{ply} also ensures a smooth transition between squeezing and bleeding flow.

The composition of η_{micro} is derived from micromechanical considerations, which do not give a precise analytical solution but provide a suitable form for the phenomenological model. To unite the formulations for the different flow types, bleeding is presented as the squeezing flow of resin along the fibres, leading to the loss of resin from the network of fibres. Hence, as opposed to conventional modelling of percolation flow by the constitutive equations of Darcy, bleeding deformation is described by Eq. (1), which considerably simplifies the modelling framework. Prior to locking, η_{micro} is determined by considering a regular approximation of the fibrous architecture in the bulk of the material (see Fig. 5a)), and assuming the squeezing of resin from between neighbouring fibres in the unit cell (the fibre cross-sections are approximated to be square for simplicity of derivation). As illustrated in Fig. 5b), upon compaction, the upper fibre in a unit cell approaches the fibre below, squeezing the resin in the transverse direction. As the gap between fibres reduces, the apparent viscosity increases. Upon geometrical locking of squeeze flow at the edges (at which the fibre packing is assumed to be square[1]), the direction of the flow changes and the resin is pushed along the fibres under bleeding flow, leading to a further increase in viscosity. The same procedure as for before locking is applied to derive the expression of η_{micro} when bleeding occurs, but now considering a squeezing flow along the fibre direction. In both

---

[1] The expression of η_{micro} only changes by a constant for different types of packing (Hubert and Poursartip, 1998). Assuming regular packing considerably eases the model derivation.

Non-homogeneous strain distribution under no-slip condition
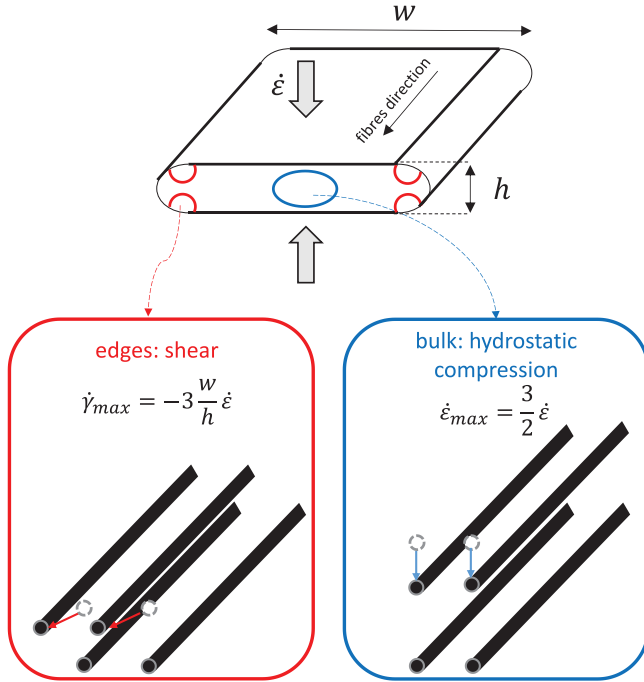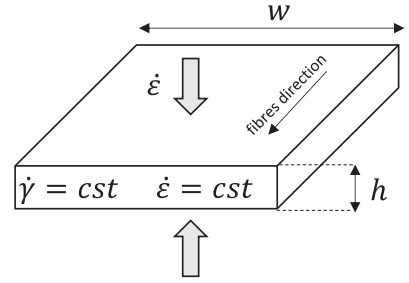
Homogenised behaviour

Fig. 4. Schematic showing model simplifications, from non-homogenious strain with shear behaviour at the tape edges and hydrostatic compression to a representative homogenised behaviour ("cst." stands for "constant"). The expressions for the maximum shear strain rate (at the edges) and the maximum through thickness strain rate (in the bulk material) follow directly from Rogers's (1989) analytical solution for the flow of an incompressible tape.

cases, Roger's analytical expression for the squeezing flow of a Newton fluid is simply rearranged considering the squeezing flow of a resin of viscosity η_{resin} between two fibres. This leads to the expressions for η_{micro} before and after locking as given in Eqs. (5a) and (5b), respectively:

$$\eta_{micro} = \eta_{resin} \cdot 2 \cdot \sqrt{\chi_l} \cdot \exp(\varepsilon) \cdot k \cdot \left(\left(\frac{k}{\sqrt{\chi_f} \exp(\varepsilon) - k} \right)^2 + 3 \right) \quad (a)$$

$$\eta_{micro} = \eta_{resin} \cdot 2 \cdot \left(\frac{l_0}{d} \right)^2 \cdot k \cdot \left(\frac{k}{\sqrt{\chi_f} \exp(\varepsilon) - k} \right)^2 \quad (b) \quad (5)$$

where l_0 is the fibre length, d is the edge length of the square fibres in the plane perpendicular to the fibre direction (d is adjusted so that the volume fraction stays the same as it would be for circular fibres) and k is a phenomenological parameter, which is defined as the product of d by the distance between fibres in the compaction direction in the initial configuration of the unit cell (a_y^i). Finally, χ_l and χ_f are the aspect ratios of a unit cell at locking and the compaction limit respectively. χ_l is defined as $\chi_l = \exp(-2\varepsilon^l)$. In order to reduce the number of parameters needed by the model, the volume fraction is estimated to be 50% in a debulked unconsolidated prepreg stack. Up to locking, the fibre volume fraction does not change and it reaches about 70% in a cured laminate. This suggests that $\chi_l \approx 0.7 \times \chi_f$.

Finally, the strain at locking, ε^l, can be obtained expressing the maximum shear rate at the ply edge ($\dot{\gamma}_{lock}$) and the

maximum through thickness strain rate in the bulk material ($\dot{\varepsilon}_{lock}$). Once again, Rogers' analytical solution for the squeezing of an incompressible Newtonian media (Rogers, 1989) is used in the first approximation to estimate this value. By subsequently integrating the strain rate as function of time in the location of maximum shear gives rise to:

$$\varepsilon^l = \max \left\{ -\ln \left(\sqrt{\frac{2}{3} \frac{h_0}{w_0} \tan(\gamma_{lock}) + 1} \right), \frac{2}{3} \varepsilon_{lock} \right\} \quad (6)$$

where γ_{lock} is the maximum shear at the ply edge which can be determined from geometrical considerations (see Annexe A.1). This departs from the previous approximation of the micro-scale geometry with regular square packing of fibre and for locking considers a state when the fibres are in contact.

3.2. Derivation of material parameters from ramp–dwell test

Three parameters need to be determined for bleeding and squeezing stages: the rate term parameters a and b defined in Eq. (5) and the parameter k in Eq. (5). Fig. 6 provides an illustration of how these parameters can be determined as well as evidence that the obtained expression is suitable for describing the experimental data over the entire range of the considered parameters. It has been found that for a given flow mode the experimental pressure–strain dependency in the entire range of strain
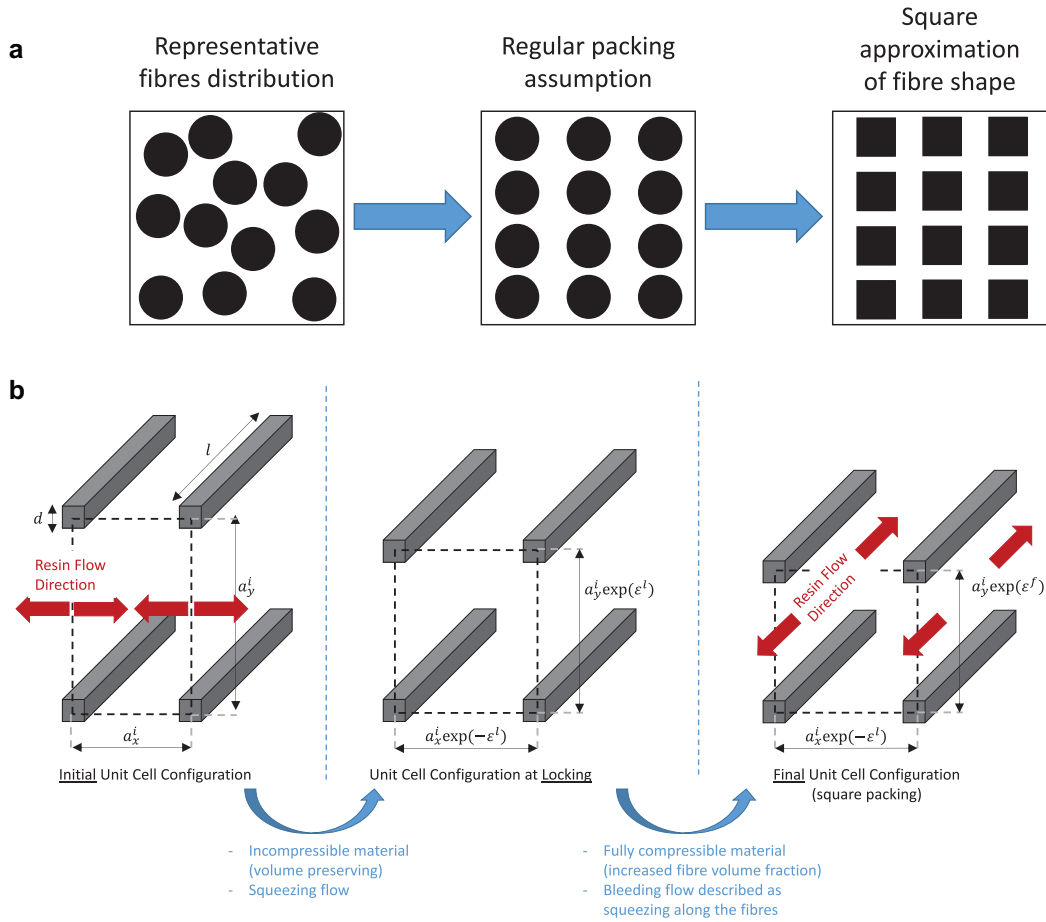
Fig. 5. Schematic representation of the main assumptions used in the derivation of the fibre scale term η_{micro}. (a) To ease the use of Roger's squeezing flow equations (Rogers, 1989), the fibre distribution is idealised to a regularly packed square fibres arrangement. (b) Prior to locking, resin flows transversely to the fibres whilst the fibre volume fraction remains constant. After locking (i.e. $|\varepsilon| > |\varepsilon^l|$), bleeding is described as resin flow along the fibres.

rates can converge to a linear function in the $\frac{\frac{\sigma}{\dot{\varepsilon}}}{\eta_{ply}\eta_{micro}}$ vs. $\dot{\varepsilon}$ log–log diagram if the value of k is properly chosen. This observation gives grounds for a procedure that allows to determine all the three constants in a simple way. At each temperature, k can be determined by varying its magnitude until all the experimental points, showing creep at various compaction levels, converge to two well determined straight lines in the afore-mentioned diagram. Parameters a and b (for simplicity sake we write: $b = \bar{b}.\ln(\eta_{res})$) can then be determined by linear regression. The procedure is conducted separately for the squeezing and bleeding flows so that for each temperature, two distinct set of parameters a and b are obtained (one for squeezing and one for bleeding). The accurate value for k at a given temperature is chosen so that the coefficient of regression of the line fitting the experimental data is as close as possible to 1. Finally, solving the ordinary differential equation presented in Eq.. (1) allows plotting the diagram presented in Fig. 6b) where the thickness vs. time evolution of one of the BP specimens is superimposed on the model prediction. The perfect match between both sets of data proves the suitability of the equations used.

The same procedure was repeated for all experiments (Nixon-Pearson et al., submitted for publication, 2015) where specimens of baseline configuration were subjected to a ramp–dwell loading. This allowed extracting parameters *a, b* and *k* for all the temperatures and specimen configuration tested. As illustrated in Fig. 7, at a given temperature, parameters extracted from the CP specimens show very little variation between repeats. Parameters extracted from BP specimens vary more from repeat to repeat and their mean value (at a given test temperature) is slightly different from the average value of CP specimens subjected to the same test conditions. The observed difference is however small enough to not consider CP and BP specimens as two distinct material systems and hence BP and CP test configuration can be described using the same set of materials parameters. The differences observed between BP and CP specimens upon compaction illustrated in Fig. 2, originate from the capacity of two plies of the same orientation in direct contact with each other to merge so that they form a new effective ply of twice the thickness. However, if the interface between the plies is not perfect (e.g. due to slight misorientation introduced during layup,
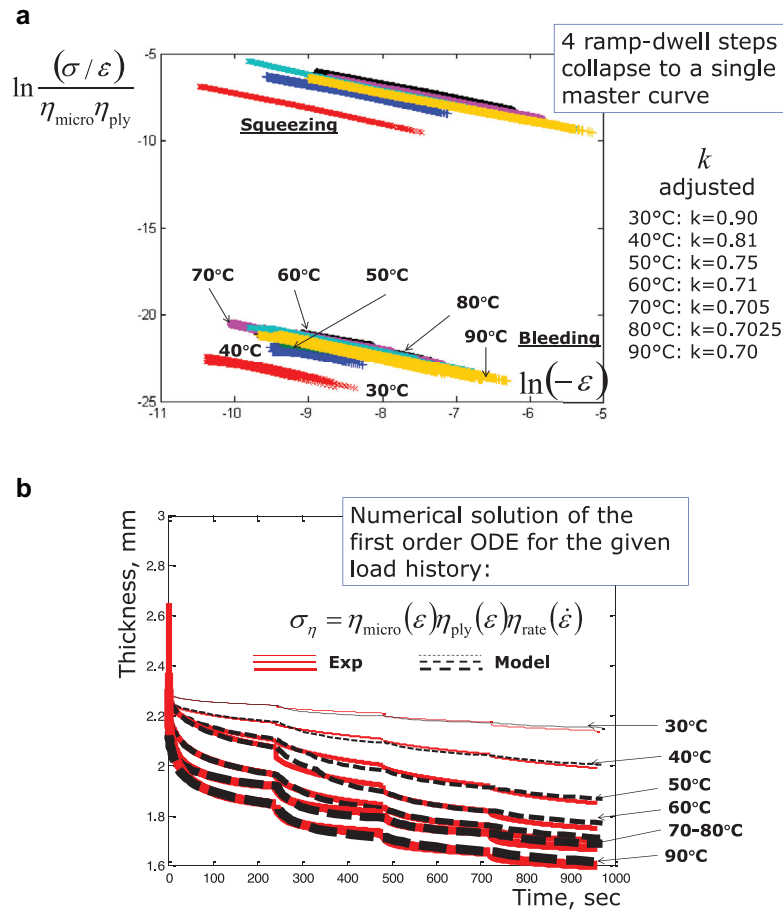
a

b

Fig. 6. (a) $\frac{\sigma/\varepsilon}{\eta_{ply}\eta_{micro}}$ vs. $\dot{\varepsilon}$ log–log diagram in BP specimens for adjusted values of the parameter k – (b) Comparison of the thickness vs time evolution of the BP specimens obtained experimentally with the model prediction after determination the 3 parameters needed by the model.

or because of the pre-preg having been kept slightly too long, etc.), the observed behaviour will be a hybrid between the behaviour of a single ply and the behaviour of a ply of twice the thickness. The variation in quality of the interface between plies of the same orientation within BP specimens probably explains the greater variation between test repeats. As there is no interaction between plies of the same orientation in a CP specimen, less variation is observed. It is very likely that if perfect interfaces could be assured, the parameters extracted (at a given temperature) from BP and CP compaction tests would converge to a single value.

Although Fig. 7 only shows the IM7-8552 material, a very similar trend is observed for the second material system tested, IMA-M21. The corresponding data are not presented here for brevity. In both cases, at each temperature, the parameters' value were defined as the average values of the considered parameter from the CP test repeats, which as discussed above allows elimination of the uncertainty linked to ply-to-ply interaction. The final values for k, a and b at the different tested temperatures and for both material systems are given in Tables 2 and 3 respectively.

4. A hyper-viscoelastic model for consolidation of uncured prepreg

4.1. Thermodynamical framework

As mentioned in the introduction, the consolidation of composite laminates prior to curing strongly influences the formation of fibre path defects (such as wrinkles Hubert et al., 1999, folds, and in-plane waviness) through the generation of excessive fibre length. Manufacturing defects in composites materials are responsible for severe reductions in mechanical properties (Bloom et al., 2013; Potter, 2009; Potter et al., 2008). Modern FE techniques are able to predict the knockdown effect induced by fibre path defects (Mukhopadhyay et al., 2015a; Mukhopadhyay et al., 2015b) but these techniques require a knowledge of the internal ply architecture of the cured laminate which is generally achieved by costly and time-consuming imaging techniques. In the present section, the 1D model that was presented above has been extended into a hyper-viscoelastic model with the aim of building a fully numerical framework for compaction prediction of uncured composite laminates, which has the potential to help in the
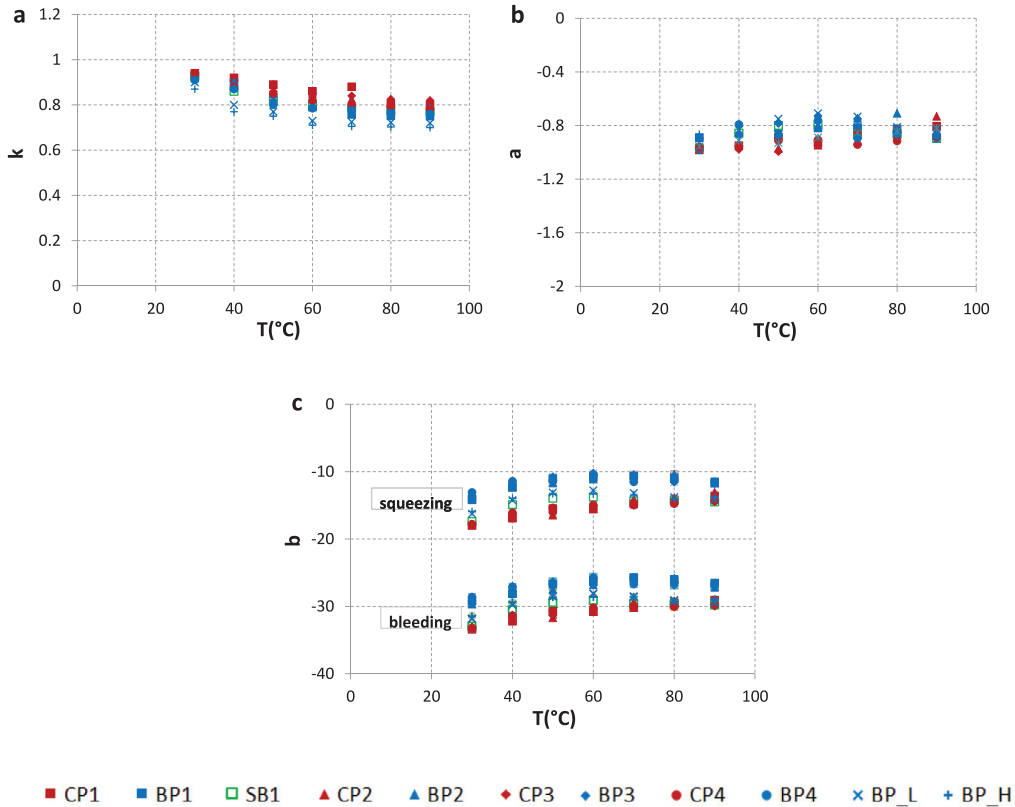
Fig. 7. Evolution of the parameters *k* (a), *a* (b) and *b* (c) as a function of temperature for the material system IM7-8552. For all temperatures, 4 CP, 1 SB and 6 BP specimens were tested.

Table 2
Model parameters values at each temperature tested for material system IM7-8552.

IM7-8552							
T (°C)	30	40	50	60	70	80	90
K	0.933	0.895	0.86	0.836	0.813	0.801	0.795
A	−0.954	−0.932	−0.909	−0.888	−0.866	−0.844	−0.822
b (squeezing)	−18.15	−16.90	−15.63	−15.18	−14.93	−14.87	−14.98
b (bleeding)	−34.88	−33.63	−32.36	−31.91	−31.66	−31.59	−31.71

Table 3
Model parameters values at each temperature tested for material system IMA-M21.

IMA-M21							
T (°C)	30	40	50	60	70	80	90
k	0.96	0.8925	0.83	0.805	0.8	0.795	0.79
a	−0.934	−0.818	−0.752	−0.731	−0.752	−0.8	−0.864
b (squeezing)	−17.89	−15.78	−14.44	−13.9	−13.84	−13.98	−14.58
b (bleeding)	−34.62	−32.51	−31.17	−30.63	−30.56	−30.70	−31.31

understanding of formation and mitigation of manufacturing defects. The thermodynamical framework first proposed by Limbert and Middleton (2004) for the description of soft biological tissues (muscles) was used. This is very relevant for the description of uncured prepreg as both materials are highly viscous and present one strong direction of anisotropy.

Following Spencer (1992), the material was described as an arrangement of fibres (characterised by a unit vector n_0, which defines locally the preferred direction from which material anisotropy arises) continuously distributed in a highly compliant solid isotropic matrix. Under the assumptions that the process considered is isothermal and that static equilibrium has been reached, Limbert and Middleton (2004) applied the First and Second Principles of Thermodynamics (which reduces to the Clausius–Duhem inequality, Truesdall and Noll, 1992) to a free energy function ψ^e which depends on the position (X) of the

material point, the right Cauchy–Green deformation tensor (C) and the structural tensor (N_0) which characterises the local directional properties of the material and is defined as $N_0 = n_0 \otimes n_0$. This leads to the expression of the general thermodynamic potential (ψ) and the Piola-Kirchhoff stress tensor (S) as the additive superposition of an elastic part related to the deformation of fibres and a viscous part related to the flow of matrix described above. The resultant expression is given by Eqs. (7) and (8) where $\dot{C}$ denotes the derivative of C with respect to the time and t is the time parameter.

$$\psi\left(X, C(X,t), \dot{C}(X,t), N_0(X)\right) = \psi^e(X, C(X,t), N_0(X))$$
$$+ \psi^v\left(X, C(X,t), \dot{C}(X,t), N_0(X)\right) \quad (7)$$

$$S = S^e + S^v = 2\left(\frac{\partial \psi^e}{\partial C} + \frac{\partial \psi^v}{\partial \dot{C}}\right) \quad (8)$$

Finally, the Cauchy stress tensor can easily be obtained by pushing-forward Eq. (8) (Mardsen and Hughes, 1994):

$$\sigma = \sigma^e + \sigma^v = \frac{2}{J}\left(F.\frac{\partial \psi^e}{\partial C}.F^T + F.\frac{\partial \psi^v}{\partial \dot{C}}.F^T\right) \quad (9)$$

In Eq. (8), σ^e and σ^v are respectively the elastic and viscous stress tensors. F and F^T are the deformation gradient and its transposal respectively and J is the determinant of the deformation gradient.

The uncoupling of the strain and the strain rate implied by Eq. (8) eases the formulation and makes the framework particularly attractive. It is also important to note that although the strain and strain rate terms are assumed to be decoupled, the viscous potential can still depend on strain. In this case, the strain is considered as a material parameter rather than a variable. Despite these simplifications, Limbert and Middleton (2004) framework stays fairly general. Hence, 17 invariants (Boehler, 1987) are required to fully describe the expression of ψ. Further simplifications are necessary and these are described in the next two sections together with the formulation of ψ^v consistent with the 1D model proposed in Section 2 of this paper.

4.2. Elastic potential

The 1D model introduced in Section 2 is purely viscous, therefore the elastic terms in Eqs. (7)–(9) are used solely to introduce the strong direction of anisotropy along the fibres (which does not appear anywhere in the 1D model). It was chosen to express ψ^e with the Neo-Hookean elastic potential for transversely isotropic material introduced by Bonet and Burton (1998) which necessitate the definition of 5 invariants (Limbert and Middleton, 2004; Bonet and Burton, 1998; Bonet and Wood, 1997). The corresponding expression for ψ^e is given in Eq. (10) and the definitions for the invariants used can be found in Eqs. (10)–(14).

$$\psi^e = \frac{1}{2}\mu_T(I_1 - 3) - \mu_T \ln(J) + \frac{1}{2}\lambda(J - 1)^2$$
$$+ \left[(\mu_T - \mu_L) + \frac{\alpha}{4}\ln(J) + \frac{\beta}{8}(I_4 - 1)\right](I_4 - 1)$$
$$+ \frac{1}{2}(\mu_T - \mu_L)(I_5 - 1) \quad (10)$$

where 1 is the second-order unit tensor, $I_1 = 1 : C$, $I_2 = \frac{1}{2}[I_1{}^2 - (1 : C^2)]$, $I_3 = J^2 = \det(C)$, $I_4 = N_0 : C$ and $I_5 = N_0 : C^2$. The material parameters α, β, λ, μ_T and μ_L in Eq. (10) can all be expressed as a function of the engineering constants (Limbert and Middleton, 2004; Abd Latif et al., 2007).

4.3. Viscous potential

The viscous part of the general thermodynamic potential is formulated so that, under pure compression in the transverse direction, the material behaves as described by Eqs. (1)–(6). Essentially this set of equations describe the behaviour of fibres immersed in a viscous media and could, in a first approximation be applied to describe the behaviour of prepreg loaded in any direction other than the fibre direction. Therefore, it is pragmatic to consider the viscous response of prepreg to be purely isotropic while the anisotropy of the entire system follows from the contribution of the elastic fibres. Under this assumption, the overall anisotropic nature of the uncured prepreg would be maintained through the superposition of the isotropic viscous response to the anisotropic elastic behaviour described in the previous section. In their paper, Limbert and Middleton (2004), narrowed the number of invariants necessary to describe the behaviour of a transversely isotropic viscous material to 2 invariants only. The isotropic assumption made here, allows reducing this further to the invariant $J_2 = \frac{1}{2}(1 : \dot{C}^2)$ alone. In order to conserve the coupling between viscosity and elasticity appearing in Eqn. (1), ψ^v is also expressed as function of the elastic invariants I_1 and I_3 (that are treated as parameters) and can finally be rewritten as: $\psi^v = \psi^v(I_1, I_3, J_2).I_1$ is the sum of the square of the eigenvalues of the deformation gradient and represents the multi-axial state of deformation within the material. I_3, on the other hand, is used to characterise the volumetric response of the material and is closely related to the degree of incompressibility (which is of great importance for the flow mechanism transition and the material conversion from a fully incompressible to a fully compressible solid).

The formulation of the viscous potential starts by rearranging Eqn. (9) (i.e. the *push-backward* operation) as:

$$\frac{\partial \psi^v}{\partial \dot{C}} = \frac{J}{2}\left(F^{-1}.\sigma^v.F^{T^{-1}}\right) \quad (11)$$

The conditions for which the 1D model has been derived are then idealised to the case of a transversely isotropic solid compacted in one of the principal directions perpendicular to the direction of anisotropy, which is assumed to be inextensible. Calling λ the stretch in the compaction direction, the (Hencky) strain and strain rate are defined respectively as $\varepsilon = \ln(\lambda)$ and $\dot{\varepsilon} = \frac{\dot{\lambda}}{\lambda}$. Noting, without loss of generality, that 1 is the compaction direction and 3 is the fibre direction, the right Cauchy strain tensor and its derivative are respectively $C = \begin{pmatrix} \lambda^2 & 0 & 0 \\ 0 & \frac{I_3}{\lambda^2} & 0 \\ 0 & 0 & 1 \end{pmatrix}$

and $\dot{\boldsymbol{C}} = \begin{pmatrix} 2\dot{\lambda}\lambda & 0 & 0 \\ 0 & -\frac{2I_3\dot{\lambda}}{\lambda^3} & 0 \\ 0 & 0 & 0 \end{pmatrix}$, giving rise to $I_1 = C_{11} + \frac{I_3}{C_{11}} +$

1 and $J_2 = \frac{1}{2}(\frac{\dot{C}_{11}}{C_{11}^2})^2((I_1 - 1)^2 - 2I_3)$.

Combining Eqs. (1), (5) and (11), allows writing:

$$\frac{\partial \psi^v}{\partial \dot{C}_{11}} = -\frac{J}{2\lambda^2} \eta_{micro}(\varepsilon)\eta_{ply}(\varepsilon)e^b(-\dot{\varepsilon})^{a+1} \qquad (12)$$

The equation of the potential that governs the viscous response of prepreg prior to locking is obtained by integrating Eq. (11) where η_{UD} and η_{ply} have been replaced by their expressions (see Eqs. (4) and (5)) written in terms of C_{11} (that acts as a parameter) and $\dot{C}_{11}$. This finally leads to:

$$\psi^v = \left(\frac{w_0}{h_0}\right)^2 \frac{\sqrt{\chi_l}}{\chi_f} \frac{4Jke^b}{(a+2)} \left(\frac{1}{I_1^s}\right)^{-\frac{3}{2}}$$
$$\times \left(\left(\frac{k}{\sqrt{I_1^s} - \frac{k}{\sqrt{\chi_f}}}\right)^2 + 3\chi_f\right) \left(\frac{1}{2[(I_1-1)^2 + 2I_3]}\right)^{\frac{a+2}{2}} J_2^{\frac{a+2}{2}}$$

$$\qquad (13)$$

where $I_1^s = \frac{1}{2}((I_1 - 1) - \sqrt{(I_1-1)^2 - 4I_3})$.

After locking, the material is assumed to become fully compressible and no further transverse expansion of the ply/tape is possible. Under these assumptions $\boldsymbol{C} = \begin{pmatrix} \lambda^2 & 0 & 0 \\ 0 & \chi_l & 0 \\ 0 & 0 & 1 \end{pmatrix}$ (where χ_l accounts for material incom-

pressibility prior to locking) and $\dot{\boldsymbol{C}} = \begin{pmatrix} 2\dot{\lambda}\lambda & 0 & 0 \\ 0 & 0 & 0 \\ 0 & 0 & 0 \end{pmatrix}$ so

that we have: $I_1 = C_{11}^2 + \chi_l + 1$ and $J_2 = \dot{C}_{11}^2$.

The same mathematical development as the one that has led to Eq. (13) is performed and the viscous potential after locking is found to be:

$$\psi^v = \left(\frac{l_{0w_0}}{dh_0}\right)^2 \frac{\chi_l}{\chi_f} \frac{4Jke^b}{(a+2)} \left(\frac{1}{I_1^b}\right) \left(\frac{k}{\sqrt{I_1^b} - \frac{k}{\sqrt{\chi_f}}}\right)^2 \left(\frac{1}{2I_1^{b2}}\right)^{\frac{a+2}{2}} J_2^{\frac{a+2}{2}}$$

$$\qquad (14)$$

where $I_1^b = I_1 - (1 + \chi_l)$.

4.4. Implementation and tangent stiffness matrix determination

The newly proposed model was implemented in Fortran as a UMAT subroutine for the implicit finite element package Abaqus/Standard. The additive decomposition of stress (see Eq. (8)) makes the implementation relatively simple as no iterative procedure (e.g. Newton–Raphson) is required at the material point level. The ply/tape dimensions (width, thickness, length) and fibre direction are given as inputs to the subroutine as material parameters. The deformation gradient at times t and $t - \Delta t$ (where Δt is the time increment) are directly provided by Abaqus.

From there, it is possible to compute the right Cauchy strain tensor and its derivative. The determination of the invariants directly follows. Finally, Eq. (9) is used together with Eq. (10) and either Eq. (13) or Eq. (14) to compute the Cauchy stress tensor. The determination of the accurate expression for the viscous potential is performed by checking if the logarithmic strain in the compaction direction is greater than the strain at locking (see Eq. (6)). When this is the case Eq. (14) is used, otherwise the viscous potential is governed by Eq. (13). The material (quasi)-incompressibility prior to locking is enforced using Lagrange multipliers.

Finally the main difficulty of the process lies in the formulation of a consistent tangent stiffness matrix to ensure good convergence (De Souza Neto et al., 2008). Noting, $\psi^v = f(I_1, I_3)J_2^{\frac{a+2}{2}}$ (which works for both expressions of ψ^v), Eq. (8) can be written:

$$\boldsymbol{S} = \boldsymbol{S}^e + 2f(I_1, I_3)\frac{\partial J_2^{\frac{a+2}{2}}}{\partial J_2} \frac{\partial J_2}{\partial \dot{\boldsymbol{C}}} = \boldsymbol{S}^e + (a+2)f(I_1, I_3)J_2^{\frac{a}{2}}\dot{\boldsymbol{C}}$$

$$\qquad (15)$$

Rearranging Eq. (15) finally leads to:

$$\mathbb{C} = \frac{\partial \Delta \boldsymbol{S}}{\partial \Delta \boldsymbol{C}} = \mathbb{C}^e + \frac{(a+2)}{\Delta t}f(I_1, I_3)J_2^{\frac{a}{2}}\left(\frac{a}{2}J_2^{-1}\dot{\boldsymbol{C}} \otimes \dot{\boldsymbol{C}} + \mathbb{I}\right)$$

$$\qquad (16)$$

where $\mathbb{C}^e = \frac{\partial \Delta \boldsymbol{S}^e}{\partial \Delta \boldsymbol{C}}$ and $\mathbb{I}$ is the 4th order symmetric identity tensor. The expression for $\mathbb{C}^e$ follows, Holzapfel et al. (1996) and Bonet (2001) and is given in Bonet and Burton (1998).

$\mathbb{C}$ in Eq. (16) relates the Piola–Kirchhoff stress tensor to the right Cauchy strain tensor. However, the Jacobian matrix in Abaqus needs to link the Kirchhoff stress ($\boldsymbol{\tau} = J\boldsymbol{\sigma}$) to the rate of deformation ($\boldsymbol{D}$), through the Jaumann objective stress rate ($\boldsymbol{\tau}^{\nabla \mathcal{J}}$) (Ji et al., 2013). The transformation of $\mathbb{C}$ into $\mathbb{C}^{ABAQUS}$ was performed using the procedure described in Prot and Skallerud (2009) resulting in:

$$\boldsymbol{\tau}^{\nabla \mathcal{J}} = J(\mathbb{C} + \mathbb{C}') : \boldsymbol{D} = J\mathbb{C}^{ABAQUS} : \boldsymbol{D} \qquad (17)$$

where $\mathbb{C}_{ijkl} = \frac{1}{J}\boldsymbol{F}_{iI}\boldsymbol{F}_{jJ}\boldsymbol{F}_{kK}\boldsymbol{F}_{lL}\mathbb{C}_{IJKL}$ (which is the result of the *push-forward* operation on $\mathbb{C}$) and $\mathbb{C}'_{ijkl} = \frac{1}{2}(\delta_{ik}\boldsymbol{\sigma}_{jl} + \delta_{il}\boldsymbol{\sigma}_{jk} + \delta_{jk}\boldsymbol{\sigma}_{il} + \delta_{jl}\boldsymbol{\sigma}_{ik})$.

5. Model verification and validation

5.1. The finite element model

The model parameters presented in Table 1 and 2 were extracted solely from compaction tests performed on baseline CP specimens. In order to verify and check the validity of the proposed approach, Finite Element (FE) models of the "baseline" and "scale-up" compaction tests were built (see Fig. 8) using Abaqus/Standard. A ply-by-ply modelling approach was used. BP and CP stacking configurations for both material systems (i.e. IM7-8552 and IMA-M21) were considered. The material parameters for the plies' viscous behaviour were set as in Tables 2 and 3. It was assumed
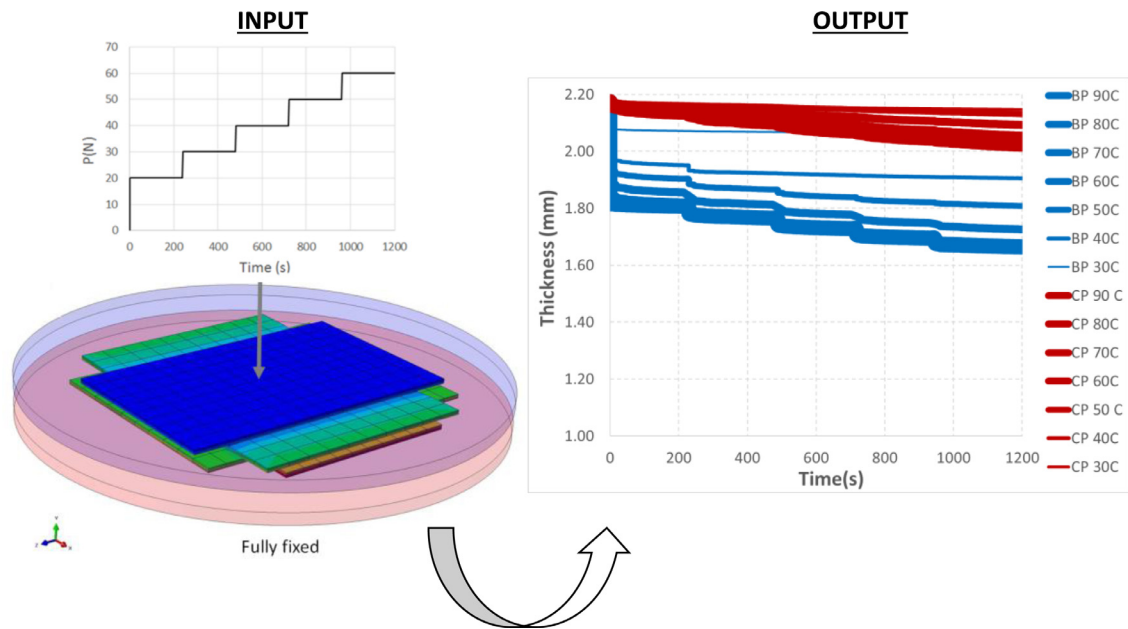
INPUT

OUTPUT

Fig. 8. Finite element simulation of a (BP) sample under ramp-dwell loading conditions. The new hyper-viscoelastic model is able to capture processing temperature as well as sample size effects.

Table 4
Elastic constants used in the FE model for the material systems IM7-8552 and IMA-M21.

E_1 (MPa)	E_2 (MPa)	E_3 (MPa)	υ_{12}	υ_{13}	υ_{23}	G_{12} (MPa)	G_{13} (MPa)	G_{23} (MPa)
25	1.0e−6	1.0e−6	0.01	0.01	0.01	0.495-6	0.495e−6	1.0

that tests were performed at isothermal conditions. Temperatures varying from 30 °C to 90 °C with a 10 °C increment were modelled by changing the material properties. The Young's modulus (E_1) in the fibre direction was adjusted (see Table 4) so as to give the correct (i.e. fairly small) bending stiffness rather than having the correct tensile stiffness, which is not relevant for wrinkling phenomena (Boisse et al., 2011). The other elastic constants were assumed to be very small but a value was still prescribed to ensure stability of the FE code (see Table 4). It was finally assumed that the elastic properties of the two material systems considered here are not significantly different prior to curing. The tape dimensions and initial fibre directions in each ply were also input as material parameters. 0.95 mm × 0.95 mm single integration point elements with hourglass control were used (one element per ply was used in the thickness direction; 0.125 mm for IM7-8552 and 0.165 mm for IMA-M21).

The two heat plates between which the samples were compacted in the Dynamic Mechanical Analysis (DMA) instrument (baseline specimen) or in the Instron universal testing machine (scale-up specimen) were modelled as rigid bodies. The bottom plate was fully fixed and the movement of the top plate was controlled through the application of a single point load at the reference point of the rigid body. A general hard contact was used as a first approximation of the tool/ply and ply/ply in-

teraction. In an attempt to capture the greater spreading behaviour of the inner ply blocks observed experimentally (Nixon-Pearson et al., submitted for publication, 2015) a slightly greater friction coefficient (i.e. 0.05) was prescribed for the tool/ply interaction than for the contact between a 0° ply with a 90° ply that was assumed to be frictionless (to allow for tape spreading). Based on experimental observations (Nixon-Pearson et al., submitted for publication, 2015) showing substantial nesting between plies of the same orientation in the ply blocks, the interaction between them was modelled using a rough contact.

5.2. Qualitative assessment

As illustrated in Fig. 8, where a graph of the predicted evolution of thickness with time for samples of different stacking sequences tested at different temperatures is presented, the newly proposed model is able to reproduce the main features of the compaction behaviour of uncured prepreg under the processing conditions used in the experimental program (Nixon-Pearson et al., submitted for publication, 2015). It is, for example, capable of capturing the existence of a compaction limit that varies with the sample geometry and testing temperature. The convergence of the compaction limit for
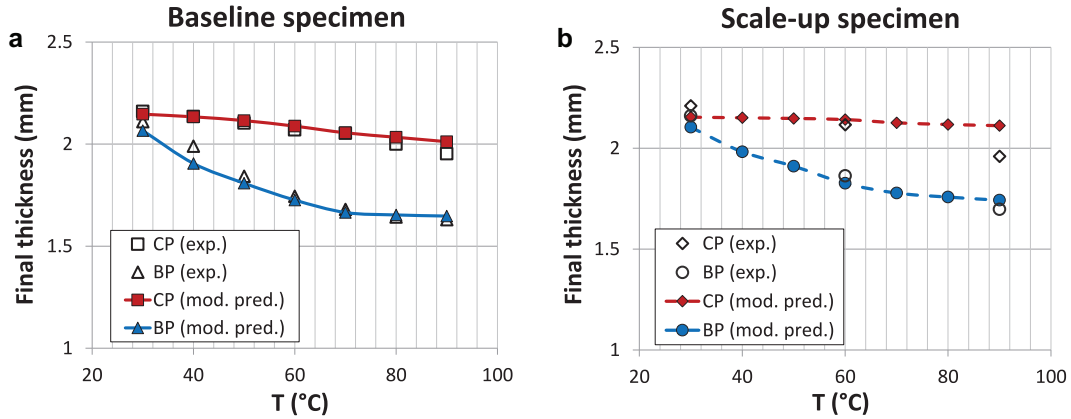
IM7-8552

Fig. 9. Variation of the samples' thickness after compaction with the testing temperature and the specimen geometry for baseline (a) and scale-up (b) specimen made of IM7-8552. Model predictions (in colour) are superimposed to average experimental values taken from (Nixon-Pearson et al., submitted for publication, 2015) (in black). (For interpretation of the references to colour in this figure legend, the reader is referred to the web version of this article).
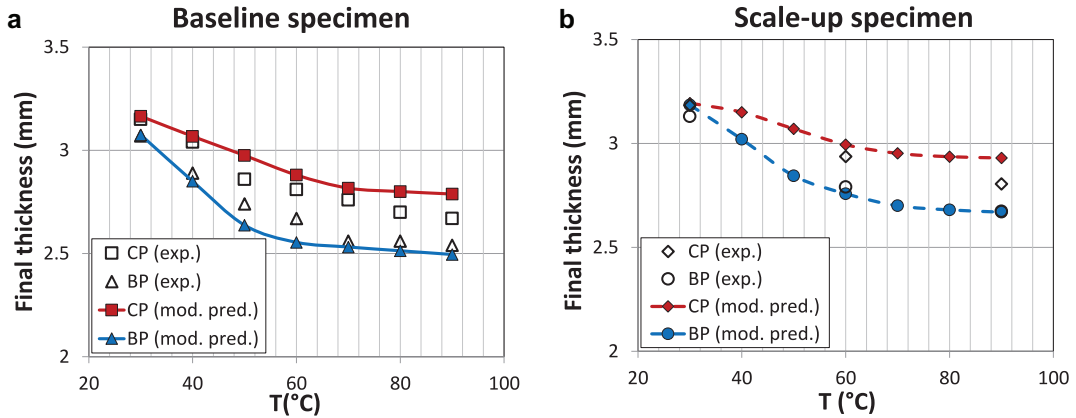
IMA-M21

Fig. 10. Variation of the samples' thickness after compaction with the testing temperature and the specimen geometry for baseline (a) and scale-up (b) specimen made of IMA-M21. Model predictions (in colour) are superimposed to average experimental values taken from Nixon-Pearson et al. (submitted for publication) and (2015) (in black). (For interpretation of the references to colour in this figure legend, the reader is referred to the web version of this article).

temperatures greater than 70 °C is also predicted by the model.

5.3. Model validation

Figs. 9 and 10 confirm the validity of the approach through a more quantitative comparison to test data. They show that, for both material systems, the new hyper-viscoelastic model is able to predict accurately the final thickness of the prepreg stacks for different stacking sequences and sample geometry within a wide range of test temperature (i.e. 30 °C–90 °C). As the viscous parameters (see Tables 1 and 2) were extracted from testing on samples of baseline geometry, the reasonably good agreements between experimental data and model predictions

for baseline test cases proves the validity of the parameter extraction procedure presented in Section 3.2 and gives a good verification of the model. Proper model validation is provided by the equally good match obtained for scale-up (i.e. doubled in-plane dimension) specimens of BP and CP configurations (that were not included in the parameter extraction procedure).

Finally, in Fig. 11, the evolution of the normalised tape spreading with different testing temperatures gives further validation of the proposed approach. The match of the experimental data with the model prediction for BP scale-up specimens ensures a good validation of the locking criterion (and underlying assumptions) presented in Eq. (5) as well as of the Lagrangian multiplier procedure enforcing incompressibility prior to locking.
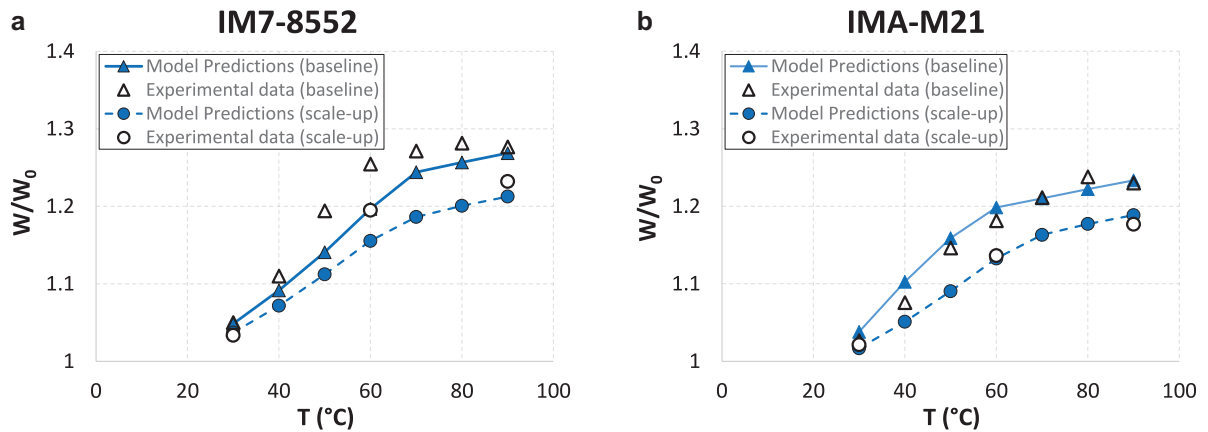
Fig. 11. Variation of the normalised width after compaction of BP samples with the test temperature for material systems IM7-8552 (a) and IMA-M21 (b). Model predictions (in blue) are superimposed to averaged experimental data (Nixon-Pearson et al., submitted for publication, 2015) (in black). (For interpretation of the references to colour in this figure legend, the reader is referred to the web version of this article).

6. Conclusion

Compaction experiments were performed on two toughened epoxy prepreg systems: IM7-8552 and IMA-M21 under processing conditions consistent with automatic fibre deposition; hot debulking and pre-curing consolidation. The experimental observations, described to a greater extend in another paper (Nixon-Pearson et al., submitted for publication, 2015), highlighted a hybrid behaviour between what is commonly observed for thermoplastic based fibre reinforced composites and typical thermoset behaviour. Hence, like thermoplastic-based systems large differences in compressibility between thick and thin samples and wide and narrow tape was observed; whilst similar to thermosets a compaction limit was reached at high temperature and high pressure levels. These experimental results also highlighted the existence of a flow transition mechanism between squeezing and bleeding flows.

Based on these observations, a new modelling framework for resin flow in uncured toughened prepreg systems at the ply scale was developed. Unlike existing models, the new phenomenological model considers both squeezing and bleeding flow. The transition between flows is realised through an assumption of the micro-mechanical behaviour of the fibres that upon squeezing that leads to rearrangement and a "locked" fibre architecture that cannot be changed upon further application of pressure. It is then assumed that after "locking" the resin can only bleed out of the system. Unlike traditional models for thermoset based systems that mostly use Dracy's law, the multiplicative decomposition of the apparent ply viscosity (Gutowski et al., 1987) into a strain dependent and a strain rate dependent term originally proposed by Kelly (2011) is assumed. This allows a smooth transition from squeezing to bleeding flow. One of the main advantages of the proposed model is that it only requires the determination of 3 material parameters at a given temperature, in addition to the already known tape dimensions that are explic-

itly present in the model formulation. It has been shown how these parameters can easily be extracted from simple compaction experiments and how the proposed equations can accurately fit the experimentally obtained compaction curves.

In a second part of the paper, the proposed model was implemented on the form of a Hyper-viscoelastic model as a UMAT subroutine for the finite element package Abaqus/Standard. A viscous potential consistent with the equations of the analytical model was derived and the corresponding consistent tangent stiffness matrix was formulated. Model validation was performed comparing experimental results and model predictions for compaction experiments performed on samples of different sizes to the ones from which the material parameters were extracted. Excellent agreement was obtained. This new model opens the way forward towards numerical prediction of fibre path defects driven by excess length creation during prepreg consolidation in toughened epoxy prepreg systems. The present model also holds potential for extension to a general 3D model for prepreg forming (Harrison et al., 2011; Guzman-Maldonado et al., 2015) but further comparison to experimental measurements would be needed to fully validate this. In this case more attention should be given to the model behaviour under in-plane shear loading.
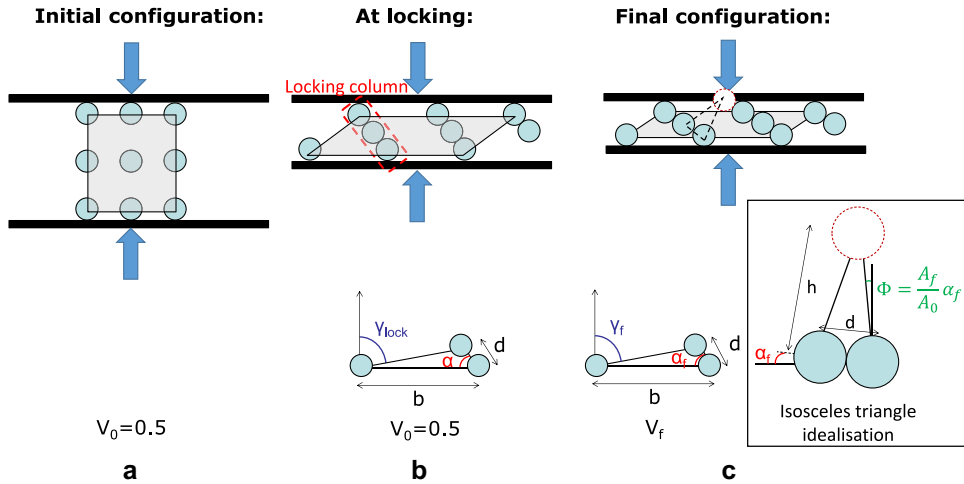
Fig. A.1. (a) An idealised square packing arrangement of fibres, (b) shear-driven squeezing and (c) bleeding.

Appendix A.1. Critical shear angle determination

The analytical expression for the maximum shear angle is obtained by considering a hypothetical micro-structure where the fibres are arranged in a perfect rectangular grid as in Fig. A.1a. The major purpose of this geometrical sketch is to capture the evolution of the average dimensions of inter-fibre channels. The regularity of the structure is a significant simplification of reality since the position of fibres in real architectures is more random, which may have important mechanical implications such as for inter-fibre friction.

A volume subjected to the maximum shear in the vicinity of a sample edge is considered. Upon incompressible compaction, the ply/tape expands by the same amount of strain by which it is compacted. At some deformation level the reconfiguration of the fibre position will close the inter-fibre channels. The fibres (initially placed diagonally with respect to each other) come into contact and so form columns, locking up the shear driven flow, Fig. A.1b. To impose further shearing, inter-fibre friction between every single fibre in the structure must therefore be overcome. Equally when neighbouring fibres approach each other the squeeze flow of resin between them causes a rapid increase in the stress required to push the fibres further together. In either case the material appears to be locked-up to further shear flow.

Due to the inhomogeneity of the through-thickness shear, lock-up at sample corners will trigger a cascade of shear-locking through the sample thickness. It can be described as the process of reduction of deformable volume. Once the entire flow front is shear locked, different scenarios can be encountered. If the resin viscosity is high, build-up of pressure may lead to explosive fibre jet-out as observed for thermoplastics by Barnes and Cogswell in the compaction of carbon-reinforced PEEK (Barnes and Cogswell, 1989). For moderate viscosity resins, flow directions may be reoriented. Resin bleeding also causes a drop in pressure and so a reduction in shear force at the flow front. For low viscosity resins, bleeding may cover the entire deforming volume, including the flow front. In this case tilting of the locking columns as sketched in Fig. A.1c may occur. No further transverse expansion is then possible and the fibre volume fraction starts decreasing. The resin flow continues until the resin pressure between the locking columns becomes so high than no more deformation is possible. For very low viscosity resin, a configuration may be reached where all the locking columns are in contact. From then on no more deformation of the fibre bed is possible and a hard limit for the fibre volume fraction has been reached. All applied pressure is reacted by the fibres which means that further bleeding is not possible. Given the extremely simplified nature of the fibre arrangements considered here, experimental characterisation of such a behaviour is extremely difficult. However, the presence of shear bands in consolidated tape laminate observed by Fast et al. (2015) through synchrotron-based X-ray tomography points in the same direction as the idealised mechanism hypothesised here.

The locking configuration appears to occur when all the fibres are in aligned contact (Fig. A.1b). Simple geometrical considerations allow for an estimation of the critical shear angle (γ_{lock}) and through-thickness strain at this condition, as a function of the fibre diameter, d, and the initial (V_0) and final (V_f) fibre volume fractions. Following the sketch of Fig. A.1, the areas of the unit cell at locking (i.e. $A_0 = \frac{\pi r^2}{2V_0}$) and at the compaction limit (i.e. $A_f = \frac{\pi r^2}{2V_f}$) are considered and after some rearrangement eqn. (A.1) is obtained:

$$\gamma_{lock} = \arcsin\left(\frac{\frac{4A_0}{d^2} - \sin(2\alpha)}{1 - \cos(2\alpha)}\right) \qquad (A.1)$$

where $\alpha = \arcsin(\frac{A_0}{A_f}\sin(\alpha_f))$ and $\alpha_f = \frac{A_0}{A_0+A_f}\arctan(\frac{d}{4A_f})$. V_0 is assumed to be 50% and, in order to keep the number of parameters as low as possible it is assumed that $V_f = k^2$ (see Tables 2 and 3). This approximation works reasonably well at temperatures greater than 50 °C (giving 60% < V_f < 70% as expected) but gives unreasonably high estimate of V_f below this temperature.

References

Abd Latif, M.J., Peric, D., Dettmer, W.G., 2007. Numerical modeling of transversely isotropic elastic material at small and finite strains. In: AIP Conference Proceedings, 909, pp. 142–146.

Balasurbramanyam, R., Jones, R.S., Wheeler, A.B., 1989. Modelling transverse flows of reinforced thermoplastic materials. Composites 20, 33–37.

Barnes, J.A., Cogswell, F.N., 1989. Transverse flow processes in continuous fibre-reinforced thermoplastic composites. Composites 20 (1), 38–42.

Bloom, L.D., Wang, J., Potter, K.D., 2013. Damage progression and defect sensitivity: an experimental study of representative wrinkles in tension. Composites Part B 45, 449–458.

Boehler, J.P., 1987. Applications of Tensor Functions in Solid Mechanics. Springer, Wien.

Boisse, P., Hamila, N., Vidal-Salle, E., Dumont, F., 2011. Simulation of wrinkling during textile composite reinforcement forming. Influence of tensile, in-plane shear and bending stiffnesses. Compos. Sci. Technol. 71, 683–692.

Bonet, J., 2001. Large strain viscoelastic constitutive models. Int. J. Solids Struct. 38 (17), 2953–2968.

Bonet, J., Burton, A.J., 1998. A simple orthotropic, transversely isotropic hyperelastic constitutive equation for large strain computations. Comput. Methods Appl. Mech. Eng. 162, 151–164.

Bonet, J., Wood, R.D., 1997. Nonlinear Solid Mechanics: A Continuum Approach for Engieeering. Cambridge University Press, London.

Christensen, R.M., 1993. Effective viscous flow properties for fibre suspensions under concentrated conditions. J. Rheol. 37 (1), 103–121.

De Souza Neto, E.A., Peric, D., Owen, D.R.J., 2008. Computational Methods for Plasticity: Theory and Applications. Wiley.

Engmann, J., Servais, C., Burbidge, A.S., 2005. Squeeze flow theory and applications to rheometry: a review. J. Non-Newton. Fluid Mech. 132, 1–27.

Fast, T., Scott, A.E., Bale, H.A., Cox, B.N., 2015. Topological and Euclidean metrics reveal spatially nonuniform structure in the entanglement of stochastic fiber bundles. J. Mater. Sci. 50 (6), 2370–2398.

Gu, Y., Li, M., Zhang, Z., Sun, Zh., 2006. Numerical simulation and experimental study on consolidation of toughened epoxy resin composite laminates. J. Compos. Mater. 40, 2257.

Gutowski, T.G., Cai, Z., Bauer, S., Boucher, D., Kingery, J., Wineman, S., 1987. Consolidation experiments for laminate composites. J. Compos. Mater. 21, 650.

Guzman-Maldonado, E., Hamila, N., Boisse, P., Bikard, J., 2015. Thermomechanical analysis, modelling and simulation of the forming of pre-impregnated thermoplastics composites. Composites Part A 48, 211–222.

Harrison, P., Yu, W.-R., Long, A.C., 2011. Rate dependent modelling of the forming behaviour of viscous textile composites. Composites Part A 42 (11), 1719–1726.

Holzapfel, G.A., Eberlein, R., Wriggers, P., Weizsäcker, H.W., 1996. Large strain analysis of soft biological membranes: formulation and finite element analysis. Comput. Methods Appl. Mech. Eng. 132 (1-2), 45–61.

Hubert, P., Johnston, A., Poursartip, A., Nelson, K., 2001. Cure kinetics and viscosity models for hexcel 8552 epoxy resin. In: Proceedings of International SAMPE Symposium and Exhibition, 46, pp. 2341–2354.

Hubert, P., Poursartip, A., 1998. A review of flow and compaction modelling relevant to thermoset matrix laminate processing. J. Reinf. Plast. Compos. 17, 286–318.

Hubert, P., Poursartip, A., 2001. Aspects of the compaction of composite angle laminates: an experimental investigation. J. Compos. Mater. 35 (2), 2–26.

Hubert, P., Poursartip, A., 2001. A method for the direct measurement of the fibre bed compaction curve of composite prepregs. Composites: Part A 32, 179–187.

Hubert, P., Vaziri, R., Poursartip, A., 1999. A two-dimensional flow model for the process simulation of complex shape composite lminates. Int. J. Numer. Methods Eng. 44, 1–26.

Ivanov, D., Li, Y., Ward, C, Potter, K., 2013. Transitional behaviour of prepregs in automated fibre deposition processes. In: Proceedings of International Conference on Cognitive Modeling. ICCM-19. Montreal, Canada.

Ji, W., Waas, A.M., Bazant, Z.P., 2013. On the importance of work-conjugacy and objective stress rates in finite deformation incremental finite element analysis. J. Appl. Mech. 80 (4).

Kaprielian, P.V., O'Neil, J.M., 1989. Shearing flow of highly anisotropic laminated composites. Composites 20 (1), 43–47.

Kelly, P.A., 2011. A viscoelastic model for the compaction of fibrous materials. J. Textile Inst. 102 (8), 689–699.

Kelly, P.A., Umer, R., Bickerton, S., 2006. Viscoelastic response of dry and wet fibrous materials during infusion processes. Composites: Part A 37, 868–873.

Li, M., Tucker III, C.L., 2002. Modelling and simulation of two-dimensional consolidation for thermoset matrix composites. Composites A 33, 877–892.

Limbert, G., Middleton, J., 2004. A transversely isotropic viscohyperelastic material application to the modeling of biological soft connective tissues. Int. J. Solids Struct. 41, 4237–4260.

Lukaszewicz, D.H.-J.A., 2011. Considerations for Automated Layup of Carbon-Fibre Thermoset Preimpregnates, (Ph.D. thesis). University of Bristol.

Mardsen, J.E., Hughes, T.J.R., 1994. Mathematical Foundations of Elasticity. Dover, New-York.

Mukhopadhyay, S., Jones, M.I., Hallett, S.R., 2015. Compressive failure of laminates containing an embedded wrinkle; experimental and numerical study. Composites Part A 73, 132–142.

Mukhopadhyay, S., Jones, M.I., Hallett, S.R., 2015. Tensile failure of laminates containing an embedded wrinkle; numerical and experimental study. Composites Part A 77, 219–228.

Nixon-Pearson O., Belnoue J.P.-H., Ivanov D., Hallett S.R., "Compaction behaviour of un-cured prepregs under processing conditions", *Journal of Composite Materials (Submitted for publication)*.

Nixon-Pearson, O.J., Belnoue, J.P.-H., Ivanov, D.S., Hallett, S.R., 2015. The compaction behaviour of uncured prepregs. In: Proceedings of the 20th International Conferemce on Composite Materials. (ICCM20). Copenhagen 2015.

Pipes, R.B., 1992. Anisotropic viscosities of an orientated fibre composite with a power law matrix. Compos. Mater. 26 (10), 1536–1552.

Potter, K.D., Khan, B., Wisnom, M., Bell, T., Stevens, J., 2008. Variability, fibre waviness and misalignment in the determination of the properties of composite materials and structures. Composites Part A 39, 1343–1354.

Potter, KD., 2009. Understanding the origins of defects and variability in composites manufacture. In: Proceedings of the 17th International Conference on Composite Materials, Edinburgh International Convention Centre. Edinburgh, UK, pp. 27–31.

Prot, V., Skallerud, B., 2009. Nonlinear solid finite element analysis of mitral valves with heterogeneous leaflet layers. Comput. Mech. 43 (3), 353–368.

Rogers, T.G., 1989. Squeezing flow of fibre-reinforced viscous fluids. J. Eng. Math. 23, 81–89.

Servais, C., Luciani, A., Månson, J.-A.E., 2002. Squeeze flow of concentrated long fibre suspensions: experiments and model. J. Non-Newton. Fluid Mech. 104, 165–184.

Shuler, S.F., Advani, S.G., 1996. Transverse squeeze flow of concentrated aligned fibers in viscous fluids. J. Non-Newton. Fluid Mech. 65, 47–74.

Spencer, A.J.M., 1992. Continuum Theory of the Mechanics of Fibre Reinforced Composites. Springer-Verlag, New-York.

Truesdall, C., Noll, W., 1992. The Non-Linear Field Theories of Mechanics. Springer-Verlag, Berlin, New-York.

Wang, E.J., Gutowski, T.G., 1991. Laps and gaps in thermoplastic composites processing. Compos. Manuf. 2 (2), 69–78.